

Giant Third-Order Nonlinear Response of Liquids at Terahertz Frequencies

Anton Tsyplkin^{1,*}, Maria Zhukova¹, Maksim Melnik¹, Irina Vorontsova¹, Maksim Kulya¹, Sergey Putilin,¹ Sergei Kozlov¹, Saumya Choudhary², and Robert W. Boyd^{2,3}

¹Laboratory of Femtosecond Optics and Femtotechnology, ITMO University, Saint-Petersburg, 197101, Russia

²The Institute of Optics, University of Rochester, Rochester, New York 14627, USA

³Department of Physics, University of Ottawa, Ottawa, Ontario K1N 6N5, Canada



(Received 26 August 2020; revised 9 February 2021; accepted 7 April 2021; published 5 May 2021)

The nonlinear response of liquids in the terahertz regime has recently attracted significant interest, even though very few measurements have been reported. Here, we report on our measurements based on a *z*-scan technique of the nonlinear refractive-index coefficient n_2 at terahertz frequencies for several liquids with noncentrosymmetric molecules, specifically, water, ethanol, and α -pinene. We describe how the value of n_2 depends on the physical parameters of these molecules. The measured values of n_2 of the liquids in the terahertz region are as much as 6 orders of magnitude larger than their corresponding values in the visible or near-IR. Through a simple theoretical model, we confirm that the predominant source of this large third-order nonlinearity is the second-order perturbative component of the vibrational response of these molecules, which have resonances in the mid-IR.

DOI: 10.1103/PhysRevApplied.15.054009

I. INTRODUCTION

Most molecules have vibrational resonances in the mid-IR that lead to a significant enhancement at terahertz frequencies of their third-order nonlinearity [1], which is characterized by the third-order susceptibility $\chi^{(3)}$ and by the coefficient of nonlinear refractive index n_2 . Recently, there has been growing interest in the use of nonlinear properties of materials as a platform for light-by-light control in the terahertz regime and therefore the characterization of nonlinearities in this frequency range is crucial. Consequently, liquids that have been shown to be sources of terahertz radiation [2–4] and display strong induced birefringence under intense terahertz radiation [5,6] are of particular importance. Earlier studies have reported on the nonlinear response in the terahertz spectral region of doped semiconductors [7] and common materials for terahertz generation and spectroscopy [8–15]. Several recent works have also reported on the large nonlinear response of liquids at terahertz frequencies [16–18].

Here, we report the explicit measurements of the second-order nonlinear refractive-index coefficient n_2 of some common liquids using the conventional *z*-scan technique [19] and we analyze how the medium parameters influence the value of n_2 . We also use the analytical model reported by Dolgaleva *et al.* [1] to theoretically calculate the vibrational contribution to the third-order nonlinear response of these liquids. Although the analytical model

described in the aforementioned work was developed for vibrational resonances in a crystal lattice, it is also suitable for an isotropic medium, such as a liquid.

The molecules of the liquids considered here—distilled water, ethanol, α -pinene, and heavy water—all lack a point of inversion symmetry. Hence, the vibration modes of these molecules themselves would have a second-order perturbative contribution. Consequently, the third-order nonlinear polarizability of the individual liquid molecule has both a second-order and a third-order perturbative component. As is the case for all media, for an incident field, the third-order perturbative contribution to the nonlinear polarizability leads to a change in the refractive index of the medium proportional to the field intensity. This response also gives rise to third-harmonic generation. The second-order nonlinear polarizability of these noncentrosymmetric molecules has two components: one that oscillates at the second harmonic of the incident field and another that oscillates at very low (dc) frequencies. The two second-order polarizabilities then interact with the incident field and lead to an effective third-order polarizability at the frequency of the incident field [see Eq. (5) in Ref. [1]] and at the third harmonic. Hence, this cascading of the second-order nonlinear response and the linear response of an individual molecule leads to a “quadratic” contribution to the third-order nonlinear polarizability. Obviously, the second-order nonlinear response vanishes on averaging the polarizability over the liquid volume. However, as the second-order nonlinear coefficients are significantly larger than their third-order

*tsyplkinan@itmo.ru

counterparts, the quadratic contribution to the third-order nonlinear response would consequently be larger than the purely third-order or “cubic” contribution.

Following a similar procedure as has been done for quartz in Ref. [1], we theoretically show that this quadratic contribution to $\chi^{(3)}$, and hence to n_2 , is about 2 orders of magnitude larger than the cubic contribution. We consider the aforementioned liquids primarily because they have vibrational absorption bands in the mid-IR. Water, being the most commonly available liquid, and ethanol are polar liquids and have very strong absorption around $2.7\ \mu\text{m}$ due to the stretching of the $-\text{O}-\text{H}$ bond. α -pinene, in turns, is an alkene and a nonpolar liquid and has a strong absorption around $3.4\ \mu\text{m}$ due to the stretching of the $-\text{C}-\text{H}$ bond. We use quasilaminar jets of these liquids for our z -scan measurements, as all three liquids have a low enough viscosity to ensure a proper flow through the jet nozzle.

II. EXPERIMENT AND RESULTS

Figures 1(a)–1(c) show the schematic of our z -scan setup. The terahertz pulse is generated by optical rectification in a $\text{MgO}: \text{LiNbO}_3$ crystal [20] of a 30-fs-long pulse with a center wavelength of 800 nm, a pulse energy of 2.2 mJ from a Ti:sapphire femtosecond laser with a regenerative amplifier. The repetition rate of the laser is 1 kHz. The intensity of the terahertz radiation is controlled by changing the IR pump intensity, as well as through crossed wire-grid polarizers. The single-cycle terahertz pulse is vertically polarized, featuring a pulse duration of 1 ps, a pulse energy of 400 nJ (a peak electric field strength of 0.27 MV/cm), and a spectrum spanning from 0.1 to 2.5 THz [for the temporal waveform and spectrum, see Fig. 1(c)]. The full width at half maximum (FWHM) of the collimated terahertz beam before the parabolic mirror PM1 is obtained by knife-edge measurements [Figs. S1(a) and S1(b) in the Supplemental Material [21]]. The values for the x and y axis are 8.5 mm and 5.6 mm, respectively. The beam is

tightly focused onto the sample by mirror PM1, with a focal length of 12.5 mm, in order to obtain a peak intensity as large as $10^8\ \text{W}/\text{cm}^2$, and then recollimated by parabolic mirror PM2, with the same focal length. The beam diameter at the focus is around 1 mm, as measured from the image of the beam at the focus [Fig. S1(c) in the Supplemental Material [21]] obtained from a terahertz camera (a Pyrocam IIIHR beam-profiling camera, with a precision of $240\ \mu\text{m}$). We note that the Rayleigh ranges for the beams along both principal axes are significantly longer than the focal length of mirror PM1. As a consequence, the foci of the beam for both principal directions coincide approximately with the geometrical focus of the mirror. Hence, the slight ellipticity ($= 1.5$) of the collimated beam should not affect the closed-aperture z -scan traces [22].

The sample liquid jet is placed within the beam and translated back and forth from the beam focus while measuring the transmitted terahertz pulse energies using a Golay cell with (without) an aperture A (transmittance of 2%) to produce the closed (open) aperture traces. The synchronization between the laser pulse and the terahertz signal detected by the Golay cell is performed using a mechanical modulator (M) placed between the lens and the Golay cell. For all the traces, the “dark signal,” obtained by blocking the terahertz beam, is subtracted from the measured terahertz signal with the sample in place. The beam profile remains unchanged on propagation through the jet, which is verified by imaging the beam on the terahertz camera with the jet switch on and then off.

A special nozzle is used to form a flat sheetlike liquid jet [23] normal to the incident terahertz field [Fig. 1(b)]. The maximum width of the jet produced by the nozzle is 8 mm and it has a thickness of 0.1 mm in its central part. The liquid-jet flow rate is adjusted such that the flow is quasilaminar and there is negligible additional evaporation into the atmosphere, which is confirmed by the absence of speckles in the interference pattern [23]. Only the upper portion of the jet is used for all the measurements shown

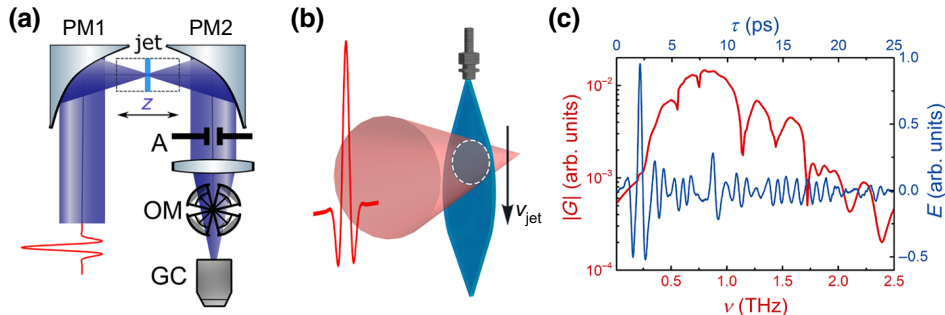


FIG. 1. (a) The schematic of the experimental setup for the z -scan measurements: PM1, PM2, parabolic mirrors; A , aperture; OM, optical modulator (chopper wheel) for synchronization, GC, Golay cell. (b) An illustration of the liquid jet obtained from the nozzle (the maximum width is 8 mm, with a thickness of 0.1 mm in the jet central part) interacting with the incident terahertz beam. (c) The temporal profile and spectrum of the generated terahertz pulse. (d)–(f) The measured closed-aperture traces (crosses) and the analytical fits (solid lines) for distilled water, α -pinene, and ethanol, respectively.

here, as the liquid jet is largely flat there [23]. The liquid from the jet is then collected in a vessel through a small screen hole (Fig. S2 in the Supplemental Material [21]), in order to prevent evaporation of the liquid from the vessel. The collected liquid is then cycled back into the jet through a pumping mechanism. We limit the translation range of our sample jet to ± 4 mm from the focus due to the divergence of our terahertz beam and the width of the jet. If the jet is placed beyond this range, spurious effects occurring due to diffraction of the diverging beam from the edge of the jet boundary come into play. Additionally, columnlike filaments at the jet edges can introduce unwanted reflections and alter the beam profile.

We note that despite our source being a broadband single-cycle pulse, our use of a z scan for the estimation of n_2 is justified due to the subwavelength thickness of the jet, for which the error in estimation of n_2 from the z -scan trace could be as low as 2%, as discussed in Ref. [24]. Essentially, the effects of dispersion and other nonlinearities, i.e., space-time focusing, self-steepening, etc., on the propagation of these broadband single-cycle pulses become significant only for sample thicknesses larger than the pulse center wavelength, for which significant errors are introduced in the estimation of n_2 from a z -scan trace under a quasimonochromatic approximation. We also note that after the first parabolic mirror, the beam has a numerical aperture equal to 1 and hence the propagation is nonparaxial. As such, it is expected that close to the focus, some of the input power will be in the longitudinal component of the field, which is at odds with the assumption of paraxial propagation for a z scan. We estimate the ratio of the power in the longitudinal field component to the transverse field component for linear propagation from the first mirror to the focus using the method shown in Ref. [25] and find it to be 7.6% (for details, see Sec. A of the Supplemental Material [21]). Since this quantity is rather small and within a reasonable margin of error, we use the conventional paraxial z -scan theory for our analysis.

One of the features of terahertz radiation is its broad spectrum. To address this point, the simulation of the focal spatirospectral distribution of single-cycle terahertz pulse

(for details, see Sec. B of the Supplemental Material [21]) is performed. The latter proves that the influence of the broadband spectrum is insignificant regarding the results obtained by the proposed z -scan technique (Fig. S6), even for a single-cycle pulse.

The measured closed-aperture z -scan traces for water, α -pinene, and ethanol, along with the analytical fits, are shown in Figs. 2(a), 2(b), and 2(c), respectively. We measure both closed- [Fig. S3(a) in the Supplemental Material [21]] and open-aperture [Fig. S3(b)] traces for all three liquids in order to take into account the nonlinear absorption, which is evident in the asymmetry between the peak and the valley in the closed-aperture trace. Since the data analysis procedure for all the liquids under consideration is similar, we only present the analysis for the water trace. An enhanced peak and a reduced valley indicate the presence of saturable absorption. To calculate n_2 , we divide the closed-aperture trace by the open-aperture trace [Fig. S3(c)] and then determine the n_2 value from the resulting trace.

For the analytical fits, we assume quasimonochromatic Gaussian pulses with a center wavelength of 0.4 mm corresponding to the peak of the terahertz spectrum [see Fig. 1(c)]. We note that in all three cases, the measured z -scan traces for the broadband source are in good agreement with the analytical quasimonochromatic fit. From the peak-to-valley variation in transmittance in the closed-aperture traces ΔT , we then determine the values of n_2 for the respective liquids using the following expression [19]:

$$n_2 = \frac{\Delta T}{0.406I_{\text{in}}} \frac{\sqrt{2}\lambda}{[2\pi L_\alpha(1-S)^{0.25}]}, \quad (1)$$

where S is the linear transmittance of the aperture, λ is the vacuum wavelength, I_{in} is the incident-beam intensity, $L_\alpha = (1 - e^{-\alpha L})/\alpha$ is the effective interaction length within the sample, with α being the absorption coefficient, and L is the jet thickness. The experimentally measured values of n_2 in the terahertz regime are $7 \times 10^{-10} \text{ cm}^2/\text{W}$ for water, $3 \times 10^{-9} \text{ cm}^2/\text{W}$ for α -pinene,

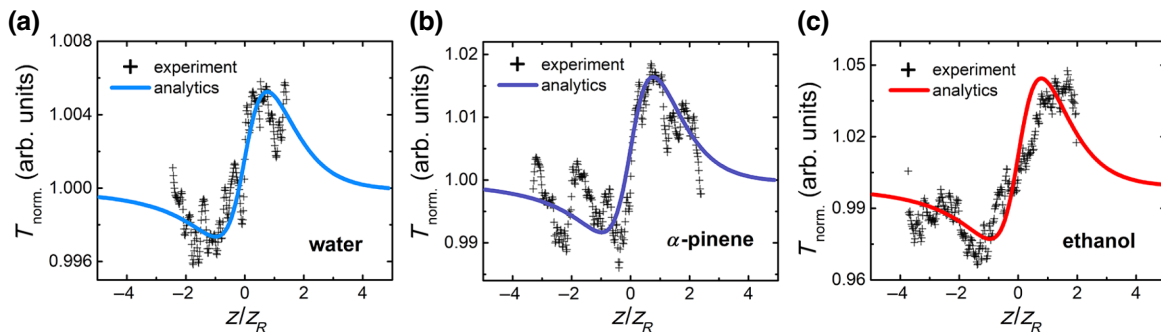


FIG. 2. The measured closed-aperture traces (crosses) and the analytical fits (solid lines) for (a) distilled water, (b) α -pinene, and (c) ethanol.

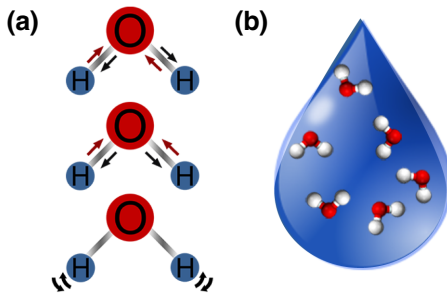


FIG. 3. (a) The different vibration modes in the water molecule. From top to bottom: asymmetric stretch, symmetric stretch, and bend. The resonances of the two stretching modes overlap with the first overtone of the bend mode around 100 THz. (b) The molecules have different orientations within the jet and the second-order nonlinear response vanishes on taking the volumetric average.

and $6 \times 10^{-9} \text{ cm}^2/\text{W}$ for ethanol. For each liquid, the measured n_2 value in the terahertz range exceeds the corresponding value in the visible and IR spectral ranges by 5–6 orders of magnitude [26–28]. The details of the analytical fits and the parameters in Eq. (1) used for the calculation of n_2 for each liquid are provided in Sec. C of the Supplemental Material [21].

III. THEORETICAL CALCULATIONS AND ANALYSIS

We now calculate the nonresonant vibrational contribution to n_2 for liquids using the analytical model described in Ref. [1]. For the intense ultrashort terahertz pulses, the main source of nonlinearity is low inertia, that is, the nonlinear response of the medium depends on the response of each molecule to the incident field. In addition, the dominant nonlinear mechanism in the terahertz spectral region is the anharmonic vibration of the individual bonds in the molecule. Any rotational transitions are suppressed in the liquid phase for these molecules. We assume the n_2 of all three liquids to be dispersionless in the spectral range under consideration. It has previously been shown in Ref. [1] that the dispersion in n_2 becomes prominent close to the two-photon resonance of the fundamental vibrational mode of the molecules, which occurs

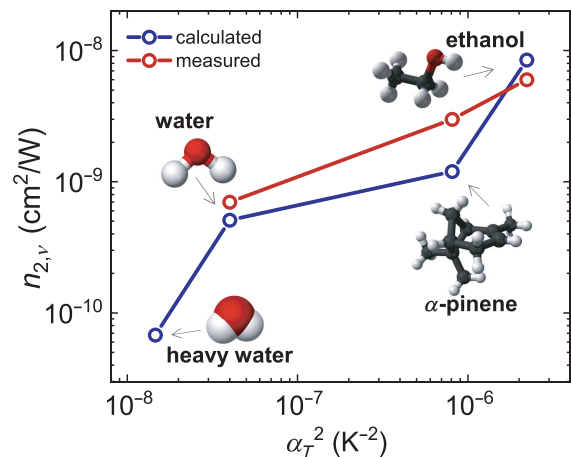


FIG. 4. The dependence of the calculated and measured values of n_2 for the four liquids on the square of their thermal expansion coefficient α_T .

at mid-IR frequencies. We specifically show, in Sec. E of the Supplemental Material [21], that for the fundamental stretching mode of the water molecule, the variation in n_2 over the spectral range of our terahertz beam is around 12%. We also note that larger molecules such as ethanol and α -pinene have multiple vibrational modes. For example, ethanol has two strong IR absorption bands close to $2.8 \mu\text{m}$. The band around $2.7 \mu\text{m}$ occurs due to the stretching of the $-\text{O}-\text{H}$ bond [for an illustration of the different stretching modes, see Fig. 3(a)] and the band around $2.9 \mu\text{m}$ has multiple structures that correspond to the stretching of the $-\text{C}-\text{H}$ bonds in the $-\text{CH}_2-$ and the $-\text{CH}_3-$ groups. In addition, there is also a very strong absorption feature around $9.6 \mu\text{m}$ due to the stretching of the $-\text{C}-\text{O}-$ bond [29]. Further, water and ethanol are polar liquids that form hydrogen bonds, which causes the $-\text{O}-\text{H}$ stretching band to red shift and more collective features in the absorption spectra due to the effect of the surrounding molecules. The restricted rotations resulting from hydrogen bonding also lead to “libration” modes at longer wavelengths than the $-\text{O}-\text{H}$ stretch band [30]. However, for simplicity, we only consider the contribution of the dominant vibration mode for each liquid, which should provide an estimate of n_2 that is correct to within an order of magnitude.

TABLE I. The parameters used for the n_2 calculations.

Liquid	Refractive indexes			
	n_{el} 800 nm	n_0 0.1–1.0 THz	α_T (K $^{-1}$)	S
Water	1.329 [31]	2.3 [32]	2×10^{-4} [33]	1
Heavy water	1.329 [27]	1.9 [34]	1.2×10^{-4} [35]	1.1 [36]
α -pinene	1.466 [37]	1.5	9×10^{-4} [38]	0.86 [39]
Ethanol	1.358 [40]	1.55 [41,42]	14.9×10^{-4} [43]	0.79 [44]

TABLE II. Nonlinear refractive-index coefficient n_2 for NIR and terahertz frequency ranges.

Liquid	NIR (cm^2/W , for comparison)	Terahertz (cm^2/W , experiment)	Terahertz (cm^2/W , calculated)		
			$n_{2,v}$	$n_{2,v}^{(1)}$	$n_{2,v}^{(2)}$
Water	1.9×10^{-16} [26]	7×10^{-10}	5×10^{-10}	5×10^{-10}	-4×10^{-14}
Heavy water	6.4×10^{-16} [27]	...	7×10^{-11}	7×10^{-11}	-2×10^{-14}
α -pinene	1.5×10^{-15} [45]	3×10^{-9}	1×10^{-9}	1×10^{-9}	-1×10^{-15}
Ethanol	7.7×10^{-16} [46]	6×10^{-9}	9×10^{-9}	9×10^{-9}	-6×10^{-15}

We use the following expression [Eq. (55) in Ref. [1]] for the calculation of n_2 modified for liquids (for details, see Sec. D of the Supplemental Material [21]):

$$\bar{n}_{2,v} = \bar{n}_{2,v}^{(1)} + \bar{n}_{2,v}^{(2)} = \frac{3a_1^2 m^2 \omega_0^4 \alpha_T^2}{32n_0 \pi^2 q^2 N^2 k_B^2} [n_{0,v}^2 - 1]^3 - \frac{9}{32\pi N n_0 \hbar \omega_0} [n_{0,v}^2 - 1]^2. \quad (2)$$

Here, a_1 is the diameter of the liquid molecule, m is the reduced mass of the vibrational mode, ω_0 is the resonance frequency of the vibrational mode, α_T is the thermal expansion coefficient, N is the number density of the molecules, n_0 is the linear refractive index, the value of q depends on the nature of the chemical bond, $n_{0,v}$ is the linear refractive-index vibrational contribution, and \hbar and k_B are the Planck and Boltzmann constants, respectively. The first and second terms on the right in Eq. (2) are the quadratic perturbative and cubic contributions, respectively. We list the values of the parameters contributing to the n_2 value assumed for all three liquids in Table I.

The calculated quadratic and cubic field contributions to n_2 , the calculated and measured total values of n_2 in the terahertz regime, and the values of n_2 at visible and IR frequencies for comparison are presented in Table I. We note that within an order of magnitude, there is very good agreement between the calculated and the measured values of n_2 for all three liquids. This indicates that the n_2 enhancement in the terahertz region is indeed due to the contribution of the nonresonant vibrational modes of the molecules. Furthermore, for all the liquids, the quadratic contribution to n_2 is several orders of magnitude larger than the cubic one. Hence, we emphasize that although the liquid itself does not have an even-order nonlinear response [see Fig. 3(b)], the quadratic perturbative nonlinear term of the noncentrosymmetric molecule makes the dominant contribution to the third-order vibrational nonlinear response.

Aside from vibrations, the following mechanisms can contribute to the third-order nonlinear response in the terahertz regime: a nonresonant electronic contribution, molecular orientation, and thermal effects. We estimate the corresponding contributions for distilled water through analytical calculations that are detailed in Sec. F of the

Supplemental Material [21]. The calculated values are as follows: the nonresonant electronic contribution $n_2^{(\text{el})} = 1.9 \times 10^{-16} \text{ cm}^2/\text{W}$, the contribution due to molecular orientation $n_2^{(\text{or})} = 6.9 \times 10^{-18} \text{ cm}^2/\text{W}$, and the thermal contribution for a cw beam $n_2^{(\text{th})} = -8 \times 10^{-3} \text{ cm}^2/\text{W}$, which when scaled by the ratio of the terahertz pulse duration (1 ps) and the thermal response time (1 s) gives an effective $n_2^{(\text{th})}$ of around $10^{-14} \text{ cm}^2/\text{W}$. All these contributions to the effective n_2 are negligible compared to the calculated and measured vibrational contributions.

Although we do not present the measured z -scan trace for heavy water, we list its parameters and the calculated n_2 value in Table II. Since the estimated n_2 value for heavy water is about an order of magnitude smaller than for regular distilled water, the nonlinear phase shift for the terahertz pulse intensity of our source is not large enough to produce a viable closed-aperture trace when the measurement errors are taken into account (see Fig. S4 in the Supplemental Material [21]).

Finally, we note from Eq. (2) that n_2 should scale with α_T^2 , as the quadratic nonlinear contribution $n_{2,v}^{(1)}$ scales with α_T^2 . In Fig. 4, we show the variation of the calculated and measured values of n_2 for all four liquids considered here with their thermal expansion coefficients squared. We find an almost linear variation in n_2 with α_T^2 , which agrees with our theoretical model for n_2 .

IV. CONCLUSION

To conclude, we report the experimental measurement of the refractive index n_2 third-order nonlinear coefficient for distilled water, ethanol, and α -pinene in the terahertz spectral region using the z -scan technique. The measured n_2 value is found to be around 5–6 orders of magnitude larger than the corresponding values at visible and IR frequencies. We propose and confirm through theoretical calculations that this significant enhancement in the third-order nonlinearity is due to the contribution of the nonresonant vibrational third-order nonlinear response of the noncentrosymmetric liquid molecules, wherein the second-order perturbative component predominates. The values of n_2 obtained from the simplified analytical model based on a single dominant vibrational mode of each molecule are close to within an order of magnitude of

the measured values and as such, are within the margin of error for z -scan measurements with a broadband pulse. We also note that the measured values of n_2 scale with the square of the thermal expansion coefficients of the liquids, which is in agreement with our theoretical model for n_2 . Finally, we underscore the significance of such a large nonlinear response from a subwavelength-thick liquid jet. Although such liquid films and jets have been used previously for terahertz generation through laser-induced plasma, the confirmation of an intrinsic large third-order nonlinearity of commonly available liquids in the terahertz spectral region may open up significant opportunities for nonlinear terahertz nonlinear optics.

ACKNOWLEDGMENTS

The work was financially supported by Russian Foundation for Basic Research (RFBR) Project No. 19-02-00154.

- [1] K. Dolgaleva, D. V. Materikina, R. W. Boyd, and S. A. Kozlov, Prediction of an extremely large nonlinear refractive index for crystals at terahertz frequencies, *Phys. Rev. A* **92**, 023809 (2015).
- [2] Y. E. Q. Jin, A. Tcypkin, and X.-C. Zhang, Terahertz wave generation from liquid water films via laser-induced breakdown, *Appl. Phys. Lett.* **113**, 181103 (2018).
- [3] I. Dey, K. Jana, V. Y. Fedorov, A. D. Koulouklidis, A. Mondal, M. Shaikh, D. Sarkar, A. D. Lad, S. Tzortzakis, A. Couairon, and G. R. Kumar, Highly efficient broadband terahertz generation from ultrashort laser filamentation in liquids, *Nat. Commun.* **8**, 1 (2017).
- [4] E. A. Ponomareva, S. A. Stumpf, A. N. Tcypkin, and S. A. Kozlov, Impact of laser-ionized liquid nonlinear characteristics on the efficiency of terahertz wave generation, *Opt. Lett.* **44**, 5485 (2019).
- [5] M. Sajadi, M. Wolf, and T. Kampfrath, Erratum: Transient birefringence of liquids induced by terahertz electric-field torque on permanent molecular dipoles, *Nat. Commun.* **8**, 1 (2017).
- [6] P. Zalden, L. Song, X. Wu, H. Huang, F. Ahr, O. D. Mücke, J. Reichert, M. Thorwart, P. K. Mishra, R. Welsch, R. Santra, F. X. Kärtner, and C. Bressler, Molecular polarizability anisotropy of liquid water revealed by terahertz-induced transient orientation, *Nat. Commun.* **9**, 1 (2018).
- [7] G. Kaur, P. Han, and X. C. Zhang, in *35th International Conference on Infrared, Millimeter, and Terahertz Waves* (IEEE, Rome, Italy, 2010). <https://ieeexplore.ieee.org/abstract/document/5613068>.
- [8] A. Woldegeorgis, T. Kurihara, B. Beleites, J. Bossert, R. Grosse, G. G. Paulus, F. Ronneberger, and A. Gopal, THz induced nonlinear effects in materials at intensities above 26 GW/cm², *J. Infrared, Millimeter, Terahertz Waves* **39**, 667 (2018).
- [9] A. N. Tcypkin, S. E. Putilin, M. C. Kulya, M. V. Melnik, A. A. Drozdov, V. G. Bespalov, X.-C. Zhang, R. W. Boyd, and S. A. Kozlov, Experimental estimate of the nonlinear refractive index of crystalline ZnSe in the terahertz spectral range, *Bull. Russ. Acad. Sci.: Phys.* **82**, 1547 (2018).
- [10] V. R. Kumar, K. C. Vardhan, K. Jana, A. D. Lad, Y. M. Ved, S. S. Prabhu, G. H. Döhler, and G. R. Kumar, in *2019 44th International Conference on Infrared, Millimeter, and Terahertz Waves (IRMMW-THz)* (IEEE, Paris, France, 2019), p. 1.
- [11] M. Cornet, J. Degert, E. Abraham, and E. Freysz, Terahertz Kerr effect in gallium phosphide crystal, *J. Opt. Soc. Am. B* **31**, 1648 (2014).
- [12] M. Sajadi, M. Wolf, and T. Kampfrath, Terahertz-field-induced optical birefringence in common window and substrate materials, *Opt. Express* **23**, 28985 (2015).
- [13] B. Wang, C. Wang, L. Wang, and X. Wu, Observation of Kerr nonlinearity and Kerr-like nonlinearity induced by terahertz generation in LiNbO₃, *Appl. Phys. Lett.* **114**, 201102 (2019).
- [14] H. A. Hafez, S. Kovalev, K.-J. Tielrooij, M. Bonn, M. Gensch, and D. Turchinovich, Terahertz nonlinear optics of graphene: From saturable absorption to high-harmonics generation, *Adv. Opt. Mater.* **8**, 1900771 (2019).
- [15] A. V. Balakin, S. V. Garnov, V. A. Makarov, N. A. Kuzeckhin, P. A. Obraztsov, P. M. Solyankin, A. P. Shkurnov, and Y. Zhu, “Terhune-like” transformation of the terahertz polarization ellipse “mutually induced” by three-wave joint propagation in liquid, *Opt. Lett.* **43**, 4406 (2018).
- [16] M. C. Hoffmann, N. C. Brandt, H. Y. Hwang, K.-L. Yeh, and K. A. Nelson, Terahertz Kerr effect, *Appl. Phys. Lett.* **95**, 231105 (2009).
- [17] S. Bodrov, Y. Sergeev, A. Murzanev, and A. Stepanov, Terahertz induced optical birefringence in polar and nonpolar liquids, *J. Chem. Phys.* **147**, 084507 (2017).
- [18] A. N. Tcypkin, M. V. Melnik, M. O. Zhukova, I. O. Vorontsova, S. E. Putilin, S. A. Kozlov, and X.-C. Zhang, High Kerr nonlinearity of water in THz spectral range, *Opt. Express* **27**, 10419 (2019).
- [19] M. Sheik-Bahae, A. Said, T.-H. Wei, D. Hagan, and E. V. Stryland, Sensitive measurement of optical nonlinearities using a single beam, *IEEE J. Quantum Electron.* **26**, 760 (1990).
- [20] J. A. Fülöp, L. Pálfalvi, S. Klingebiel, G. Almási, F. Krausz, S. Karsch, and J. Hebling, Generation of sub-mJ terahertz pulses by optical rectification, *Opt. Lett.* **37**, 557 (2012).
- [21] See the Supplemental Material at <http://link.aps.org supplemental/10.1103/PhysRevApplied.15.054009> for further details and derivations, includes Refs. [47–52].
- [22] S. M. Mian, B. Taheri, and J. P. Wicksted, Effects of beam ellipticity on z -scan measurements, *J. Opt. Soc. Am. B* **13**, 856 (1996).
- [23] A. Watanabe, H. Saito, Y. Ishida, M. Nakamoto, and T. Yajima, A new nozzle producing ultrathin liquid sheets for femtosecond pulse dye lasers, *Opt. Commun.* **71**, 301 (1989).
- [24] M. Melnik, I. Vorontsova, S. Putilin, A. Tcypkin, and S. Kozlov, Methodical inaccuracy of the z -scan method for few-cycle terahertz pulses, *Sci. Rep.* **9**, 1 (2019).
- [25] D. A. Kislin, M. A. Knyazev, Y. A. Shpolyanskii, and S. A. Kozlov, Self-action of nonparaxial few-cycle optical waves in dielectric media, *JETP Lett.* **107**, 753 (2018).
- [26] Z. Wilkes, S. Varma, Y.-H. Chen, H. Milchberg, T. Jones, and A. Ting, Direct measurements of the nonlinear index

- of refraction of water at 815 and 407 nm using single-shot supercontinuum spectral interferometry, *Appl. Phys. Lett.* **94**, 211102 (2009).
- [27] M. J. Weber, *Handbook of Optical Materials* (CRC Press, Boca Raton, 2018).
- [28] P. P. Markowicz, M. Samoca, J. Cerne, P. N. Prasad, A. Pucci, and G. Ruggeri, Modified *z*-scan techniques for investigations of nonlinear chiroptical effects, *Opt. Express* **12**, 5209 (2004).
- [29] E. Plyler, Infrared spectra of methanol, ethanol, and *n*-propanol, *J. Res. Natl. Bureau Stand.* **48**, 281 (1952).
- [30] M. F. Chaplin, Structure and properties of water in its various states, *Encycl. Water: Sci. Technol. Soc.* 1 (2019).
- [31] G. M. Hale and M. R. Querry, Optical constants of water in the 200-nm to 200- μ m wavelength region, *Appl. Opt.* **12**, 555 (1973).
- [32] L. Thrane, R. Jacobsen, P. U. Jepsen, and S. Keiding, THz reflection spectroscopy of liquid water, *Chem. Phys. Lett.* **240**, 330 (1995).
- [33] G. S. Kell, Precise representation of volume properties of water at one atmosphere, *J. Chem. Eng. Data* **12**, 66 (1967).
- [34] H. Yada, M. Nagai, and K. Tanaka, Origin of the fast relaxation component of water and heavy water revealed by terahertz time-domain attenuated total reflection spectroscopy, *Chem. Phys. Lett.* **464**, 166 (2008).
- [35] Volumetric—or cubic thermal expansion, accessed: 2020-08-20. https://www.engineeringtoolbox.com/volumetric-temperature-expansion-d_315.html.
- [36] Deuterium oxide, accessed: 2020-08-20. https://www.chemicalbook.com/ChemicalProductProperty_EN_CB3736883.htm.
- [37] M. J. O’Neil, A. Smith, P. E. Heckelman, and S. Budavari, Fundamental Physical and Mathematical Constants, in *The Merck Index—An Encyclopedia of Chemicals, Drugs, and Biologicals* (Whitehouse Station, NJ: Merck & Co., Inc.), **767**, 4342 (2001).
- [38] A. Wypych and G. Wypych, in *Databook of Solvents* (Elsevier, 2019), p. 17. <https://doi.org/10.1016/b978-1-927885-45-1.50005-8>.
- [39] Drug information—alpha-pinene, accessed: 2020-08-20. <https://druginfo.nlm.nih.gov/drugportal/name/alpha-Pinene>.
- [40] J. Rheims, J. Köser, and T. Wriedt, Refractive-index measurements in the near-IR using an Abbe refractometer, *Meas. Sci. Technol.* **8**, 601 (1997).
- [41] G. J. Wilmink, B. L. Ibey, T. Tongue, B. Schulkın, N. Laman, X. G. Peralta, C. C. Roth, C. Z. Cerna, B. D. Rivest, J. E. Grundt, and W. P. Roach, Development of a compact terahertz time-domain spectrometer for the measurement of the optical properties of biological tissues, *J. Biomed. Opt.* **16**, 047006 (2011).
- [42] Y. Yomogida, Y. Sato, R. Nozaki, T. Mishina, and J. Nakahara, Comparative dielectric study of monohydric alcohols with terahertz time-domain spectroscopy, *J. Mol. Struct.* **981**, 173 (2010).
- [43] T. F. Sun, C. A. T. Seldam, P. J. Kortbeek, N. J. Trappeniers, and S. N. Biswas, Acoustic and thermodynamic properties of ethanol from 273.15 to 333.1 5 k and up to 280 MPa, *Phys. Chem. Liq.* **18**, 107 (1988).
- [44] C. E. Wyman and N. D. Hinman, Ethanol, *Appl. Biochem. Biotechnol.* **24–25**, 735 (1990).
- [45] S. Huang, P. C. Ashworth, K. W. Kan, Y. Chen, V. P. Wallace, Y. ting Zhang, and E. Pickwell-MacPherson, Improved sample characterization in terahertz reflection imaging and spectroscopy, *Opt. Express* **17**, 3848 (2009).
- [46] P. P. Ho and R. R. Alfano, Optical Kerr effect in liquids, *Phys. Rev. A* **20**, 2170 (1979).
- [47] S. A. Kozlov, A. A. Drozdov, K. Dolgaleva, and R. W. Boyd, in *2015 40th International Conference on Infrared, Millimeter, and Terahertz waves (IRMMW-THz)* (IEEE, Hong Kong, China, 2015), p. 1. <https://doi.org/10.1109/IRMMW-THz.2015.7327741>.
- [48] T. Bowman, M. El-Shenawee, and L. K. Campbell, Terahertz transmission vs reflection imaging and model-based characterization for excised breast carcinomas, *Biomed. Opt. Express* **7**, 3756 (2016).
- [49] R. W. Boyd, in *Nonlinear Optics* (Elsevier, 2008), p. 561. <https://doi.org/10.1016/b978-0-12-369470-6.00013-7>.
- [50] X. Ge and D. Lu, Molecular polarizability of water from local dielectric response theory, *Phys. Rev. B* **96**, 075114 (2017).
- [51] N. Arnaud and J. Georges, Investigation of the thermal lens effect in water-ethanol mixtures: Composition dependence of the refractive index gradient, the enhancement factor and the Soret effect, *Spectrochim. Acta Part A: Mol. Biomol. Spectrosc.* **57**, 1295 (2001).
- [52] D. K. George and A. G. Markelz, in *Terahertz Spectroscopy and Imaging* (Springer, Berlin, Berlin, 2012), p. 229. https://doi.org/10.1007/978-3-642-29564-5_9.

Supplemental material: Giant third-order nonlinear response of liquids at terahertz frequencies

Anton Tsyplkin,* Maria Zhukova, Maksim Melnik, Irina Vorontsova, Maksim Kulya, Sergey Putilin, and Sergei Kozlov
*Laboratory of Femtosecond Optics and Femtotechnology,
ITMO University, Saint-Petersburg, 197101, Russia*

Saumya Choudhary
The Institute of Optics, University of Rochester, Rochester, NY 14627, USA

Robert W. Boyd
*Department of Physics, University of Ottawa, Ottawa, Ontario K1N 6N5, Canada
The Institute of Optics, University of Rochester, Rochester, NY 14627, USA*

(Dated: April 16, 2021)

The supplemental material presented includes the experimental characteristics and description of the data processing method used in the experiment, as well as the details regarding the way the non-paraxiality non-paraxiality and the broad spectrum of the THz field affect the z-scan measurement. Here we also provide the discussion of the theoretical derivation of the mechanisms that can contribute to the third-order nonlinear response in the THz regime, mentioned in the main text.

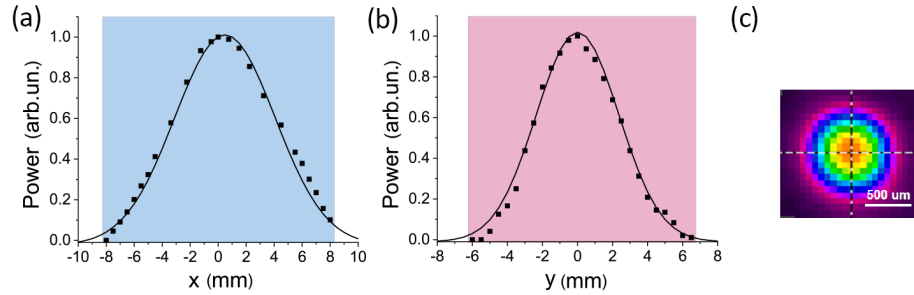


FIG. S1. The collimated THz beam profiles along the (a) x and (b) y axis obtained by knife-edge scans. The solid curves are fitted by the Gaussian function. (c) Photo of a THz beam at the focus obtained by a Pyrocam IIIHR Beam Profiling Camera.

* tsyplkinan@itmo.ru

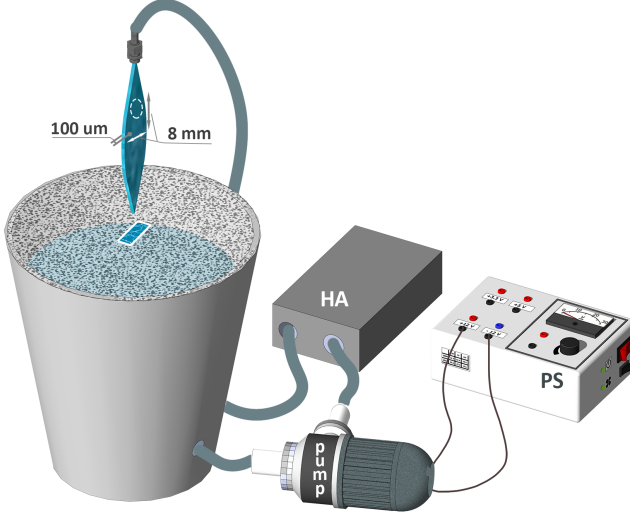


FIG. S2. Scheme of the liquid jet and circular pump system. HA denotes the hydro-accumulator, and PS the power supply.

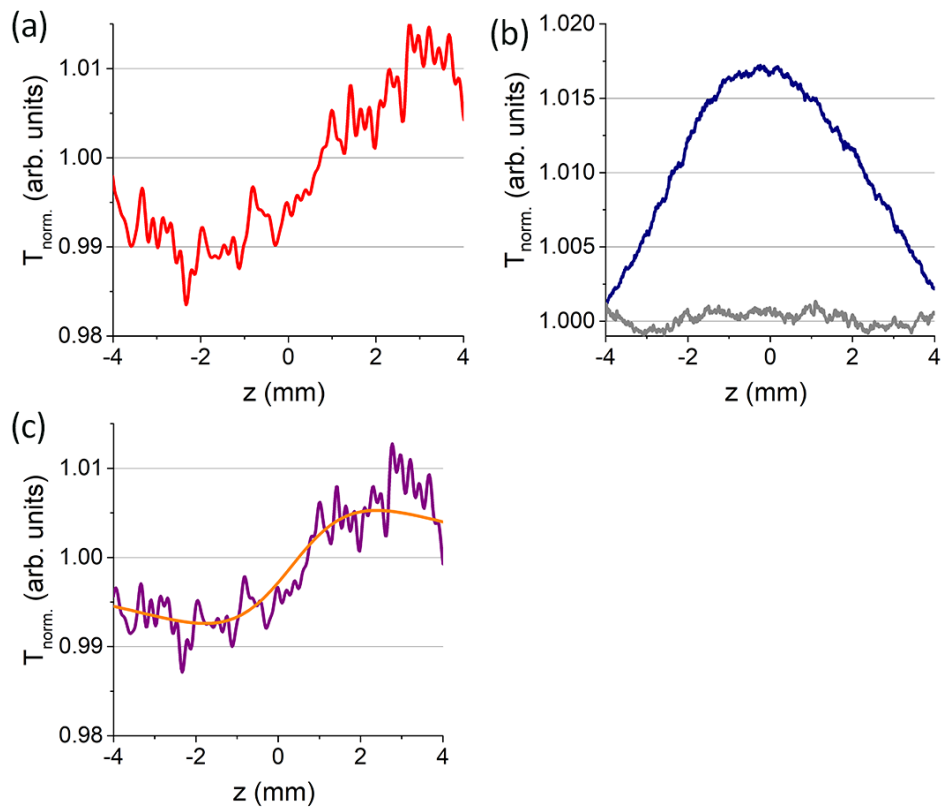


FIG. S3. Closed (a) and (b) open aperture z-scan traces for distilled water (gray line - the open aperture trace with low energy) . (c) The trace obtained by dividing the closed aperture with the open aperture trace (purple) has a symmetric peak and valley. The orange line is the analytical fit to the resulting trace, and is calculated from the standard z-scan theory for quasi-monochromatic pulses centered at a wavelength 0.4 mm.

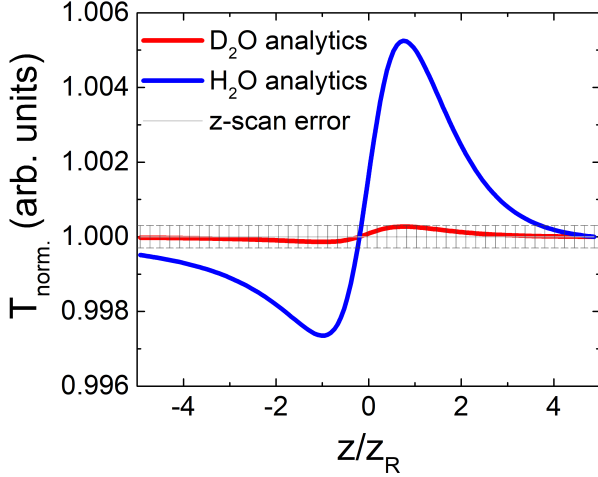


FIG. S4. The analytical z-scan curves for heavy water (red) and distilled water (blue) assuming the theoretical values of n_2 reported in **Table1** for either liquid. For heavy water the peak-to-valley variation in transmittance lies within the approximate error bars for the setup.

A. The effect of non-paraxiality of the THz beam on z-scan

Here we estimate the relative amplitudes of the transverse and the longitudinal components of the electric field of the THz beam at the focus after the first parabolic mirror PM_1 . The nonlinear propagation within the samples is not considered. We use the fully spectral approach for linear non-paraxial propagation, used for propagation within linear and weakly nonlinear media for short pulses with arbitrary temporal and spatial profiles previously [1].

Fig.S5(a) shows the beam electrical field transverse component $E_x(x, y, t)$ spatio-temporal profile at the mirror PM_1 , which has a Gaussian form featuring beam diameter of 25.4 mm. Fig.S5(b) shows the electric field after the defocusing introduced by the mirror, approximated by a thin lens with a focal length ' f' of 12.75 mm, and given by

$$\Phi(x, y) = \exp \left[-\frac{ik}{2f} (x^2 + y^2) \right] \quad (1)$$

multiplied by the field.

Fig.S5(c) and Fig.S5(d) illustrates the beam electrical field longitudinal component $E_z(x, y, t)$ spatio-temporal profile before and after the application of the defocusing at the parabolic mirror, respectively.

The tight focusing regime is obtained since the focal length f is smaller than the beam diameter, as shown in Fig.S5(e). This leads to the non-paraxial nature of propagation. In such case the following angular spectrum propagators for the transverse and the longitudinal field components are used, as given in the equation set (30) in [1]:

$$\begin{cases} g_{x,y}(\omega, k_x, k_y, z) = C_{x,y}(\omega, k_x, k_y) e^{-i\sqrt{k^2 - k_x^2 - k_y^2}z} \\ g_z(\omega, k_x, k_y, z) = \frac{k_x C_x(\omega, k_x, k_y) + k_y C_y(\omega, k_x, k_y)}{\sqrt{k^2 - k_x^2 - k_y^2}} e^{-i\sqrt{k^2 - k_x^2 - k_y^2}z} \end{cases} \quad (2)$$

where C_x and C_y constants are determined from the boundary conditions.

Fig.S5(g) and Fig.S5(h) depict $E_z(x, y, t)$, and $E_x(x, y, t)$ spatio-temporal profiles at the focus after non-paraxial propagation. We use the Fresnel propagator for transverse field component paraxial propagation as given in equation (33) in [1]:

$$g_{x,y}(\omega, k_x, k_y, z) = C_{x,y}(\omega, k_x, k_y) e^{-ikz \left(1 - \frac{k_x^2 + k_y^2}{2k^2} \right)} \quad (3)$$

Fig.S5(f) shows $E_x(x, y, t)$ spatio-temporal profile at the focus after paraxial propagation.

The ratio of energy of the field longitudinal component to the transverse one at the focus is given by

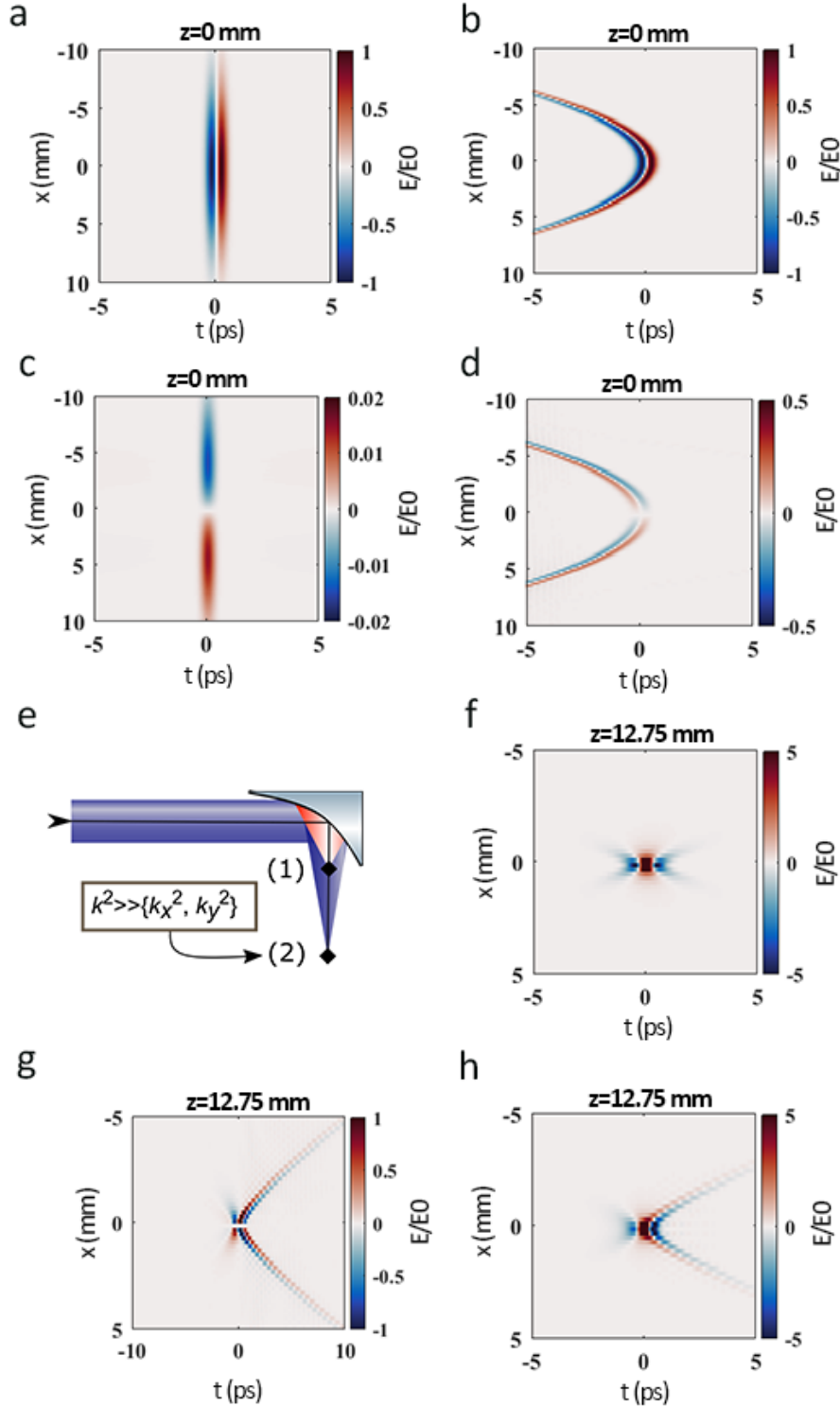


FIG. S5. Spatio-temporal evolution of the THz wave electric field for non-paraxial and paraxial propagation from PM_1 mirror to the focal plane. The electric field before the mirror and after applying the parabolic mirror defocusing for the transverse (a-b) and longitudinal (c-d) components, respectively. (e) Illustration of nonparaxial (1) and paraxial (2) focusing. (g) The longitudinal component E_z after non-paraxial propagation. (f),(h) Electric field profile at the focus for the transverse component E_x after paraxial and non-paraxial propagation, correspondingly.

$$W = \frac{\int_{-\infty}^{+\infty} \int_{-\infty}^{+\infty} \int_{-\infty}^{+\infty} |E_z(x, y, t)|^2 dx dy dt}{\int_{-\infty}^{+\infty} \int_{-\infty}^{+\infty} \int_{-\infty}^{+\infty} |E_x(x, y, t)|^2 dx dy dt} = 7.6\% \quad (4)$$

B. The role of the broad spectrum of the initial single-cycle THz pulse

We have performed the simulation of focusing of single-cycle THz pulse (Fig. S6-a) with corresponding spectrum in the range of 0.1-2.5 THz (Fig. S6-b). The spatio-spectral representation of the THz beam profile before focusing and in focal plane is presented in (Fig. S6-c) and (Fig. S6-d) correspondingly. To analyze the focused beam (d), the two cross-sections for 0.5 THz and 2 THz were additionally plotted (see (Fig. S6-e)). From these cross-sections one can observe that they differ in the low- and high-frequency tails, which proves the fact that the focal spatio-spectral distribution features a slightly arrow-like form.

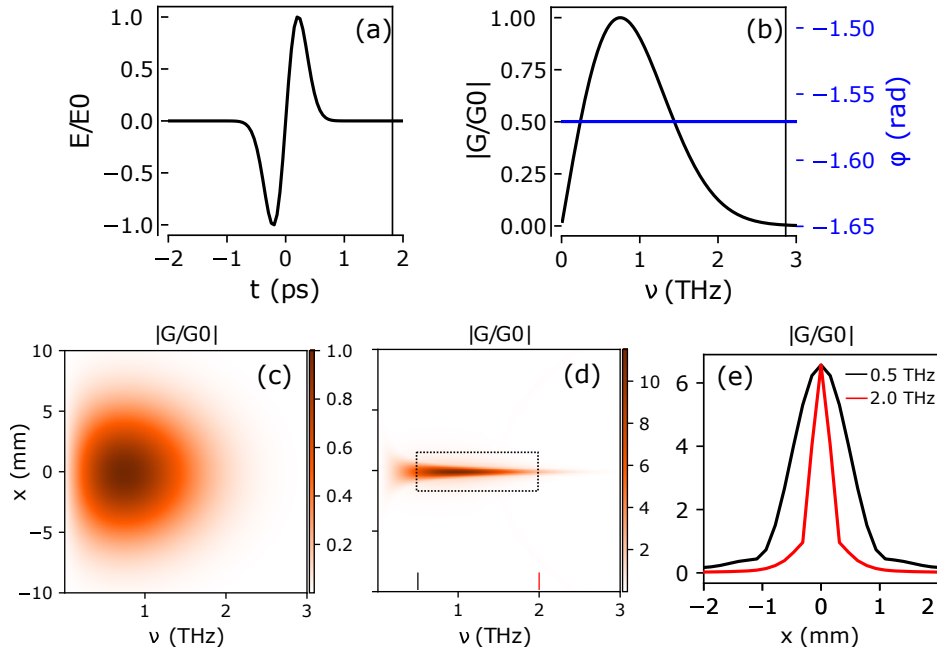


FIG. S6. (a-b) Temporal and spectral forms of the initial single-cycle THz pulse. (c-d) Spatio-spectral distribution of THz beam in plane $z = 0$ mm and in the focal plane $z = 12.75$ mm. (e) illustrates the cross-sections of (d) at 0.5 THz (black line) and 2 THz (red line).

For our calculations of n_2 from the z-scan curves, we have used the time-averaged intensity for a Gaussian pulse [2]. We do note that due to spatio-temporal propagation effects, as shown in Figs. Fig. S6-d and Fig. S6-e, the beam width - and consequently the intensity - varies considerably across the frequency spectrum of the THz pulse. Since the nonlinear index change (Δn_ν) at a given frequency is proportional to the beam intensity at that frequency, we can compare (Δn_ν) at two different frequencies within the pulse spectrum. We choose the frequencies $\nu_1 = 0.5$ THz and $\nu_2 = 2$ THz at the two ends of the pulse spectrum with similar spectral amplitudes (Fig. S6-d). As such, (Δn_ν) is inversely proportional to the square of the beam diameters at the respective frequencies. So we can write

$$\frac{n_2^{\nu_2}}{n_2^{\nu_1}} = \frac{S_{\nu_1}}{S_{\nu_2}} = \frac{d_{0.5 \text{ THz}}^2}{d_{2 \text{ THz}}^2} = \frac{1.44}{0.16} = 9 \quad (5)$$

which is within an order of magnitude. This coarse estimation of course does not take into account the spectral shape of the pulse at the focal plane. We have followed a simplistic procedure here for estimating n_2 to within an order of magnitude. Including the effects of spatio-temporal propagation in the estimation of nonlinearity through the use of z-scan with few-cycle pulses is beyond the scope of this work.

C. Calculation of the analytical z-scan traces

To calculate the analytical z-scan traces, we assume the field to be a quasi-monochromatic Gaussian pulse having a center wavelength of 0.4 mm. To calculate the transmittance through the aperture placing sample within the beam the following equation [2] is used

$$T(z) = \frac{\int_{-\infty}^{+\infty} P_T(\Delta\Phi_0(t))dt}{S \times \int_{-\infty}^{+\infty} P_i(t)dt} \quad (6)$$

where $P_i(t) = (\pi w_0^2 I_0(t))/2$ is the input pulse power, $S = 1 - \exp(-2r_a^2/w_a^2)$ is linear aperture transmittance, and $P_T(\Delta\Phi_0(t))$ is the transmitted power through the aperture given by

$$P_T(\Delta\Phi_0(t)) = c\epsilon_0 N_0 \pi \int_0^{r_a} a |E_a(r, t)|^2 r dr \quad (7)$$

where

$$\begin{aligned} E_a(r, t) &= E(z, r = 0, t) \cdot \exp\left(\frac{-\alpha L}{2}\right) \times \sum_{m=0}^{+\infty} \frac{[i\Delta\phi_0(z, t)]^m}{m!} \frac{w_{m0}}{w_m} \exp\left(-\frac{r^2}{w_m^2} - \frac{ikr^2}{2R_m} + iQ_m\right) \\ E(z, r = 0, t) &= E_0 \exp(-2t^2/\tau_0^2) \sin(\omega_0 t) w_0 / w(z) \\ \Delta\phi_0(z, t) &= \Delta\Phi_0(t) / (1 + z^2/z_0^2) \\ \Delta\Phi_0(t) &= k\Delta n_0(t)L \end{aligned} \quad (8)$$

We assume the following parameters for the different liquids: absorption coefficient α for water is taken to be 100 cm^{-1} , 10 cm^{-1} for α -pinene, and 60 cm^{-1} for ethanol; the sample length L is 0.1 mm; the THz pulse duration τ_0 is 1 ps; the central radiation frequency ω_0 is 0.75 THz; the waist radius w_0 is 0.5 mm, the aperture radius r_a is 1.5 mm, the radius of the THz beam at the mirror w_a is 12.5 mm, and the peak intensity at the beam axis I_0 is $0.5 \times 10^8 \text{ W/cm}^2$. It should be noted that the linear transmittance of the aperture is taken to be 2%, same as in the experiment, which allows us to maximize the sensitivity of the measurement, while reducing the signal-to-noise ratio.

D. Theoretical calculation of the vibrational contribution to the n_2 of liquids

We now use the classical model of an anharmonic oscillator to derive the vibrational contribution to the nonlinear refractive index coefficient n_2 of liquids with non-centrosymmetric molecules [3], and write

$$\ddot{x} + \omega_0^2 x + \beta x^2 + \gamma x^3 = \alpha E \quad (9)$$

Here, E is the electric field strength of the incident THz field, x denotes the normal mode coordinate for the dominant vibrational mode of the molecule, ω_0 is the corresponding vibrational resonance, and (α, β, γ) are the parameters characterizing the anharmonicity of the harmonic oscillator. This anharmonicity of molecular vibrations, an example of which is shown in Fig.S2(a) for the water molecule, is responsible for the nonlinear response of the molecule.

The total polarization P of the liquid medium including both the linear as well as the nonlinear terms is given by

$$\begin{aligned} P &= \frac{1}{2} N \langle p_\omega e^{i\omega t} + p_{2\omega} e^{i2\omega t} + p_{3\omega} e^{i3\omega t} + c.c. \rangle \\ \langle p_{2\omega} e^{i2\omega t} + c.c. \rangle &\approx 0 \end{aligned} \quad (10)$$

where p_{ω_i} is the spectral amplitude of the dipolar response at frequency ω_i , $\langle \rangle$ denotes the averaging over volume and molecular orientation (see Fig.S2(b)), ω is the frequency of the incident THz field, q is the charge of the chemical bond, and N is the number density of the molecules.

The polarization at the fundamental frequency has linear as well as third-order field contributions, and can be written as [3]

$$\begin{aligned} P_\omega &= \chi_\nu E_\omega + \chi_\nu^{(3)} |E_\omega|^2 E_\omega \\ \chi_\nu(\omega) &= qN \frac{\alpha}{\omega_0^2 - \omega^2} \\ \chi_\nu^{(3)}(\omega) &= \frac{qN}{4} \left[\frac{\alpha^3 \beta^2 (3\omega_0^2 - 8\omega^2)}{\omega_0^2 (\omega_0^2 - 4\omega^2)(\omega_0^2 - \omega^2)^4} - \frac{3\alpha^3 \gamma}{(\omega_0^2 - \omega^2)^4} \right] \end{aligned} \quad (11)$$

In the above expression for the third-order vibrational susceptibility $\chi_\nu^{(3)}(\omega)$, the first (second) term on the right is the second (third)-order perturbative contribution. The refractive index of the medium is given by

$$\tilde{n}(\omega) = n(\omega) + \frac{1}{2} n_2(\omega) |E|^2 \quad (12)$$

where $n(\omega)$ is the linear refractive index of the medium. We use the relation between susceptibility and refractive index

$$n = 4\pi\chi \quad (13)$$

to get

$$\begin{aligned} n_{2\nu}(\omega) &= \frac{\pi q N}{n} \left[\frac{\alpha^3 \beta^2 (3\omega_0^2 - 8\omega^2)}{\omega_0^2 (\omega_0^2 - 4\omega^2)(\omega_0^2 - \omega^2)^4} - \frac{3\alpha^3 \gamma}{(\omega_0^2 - \omega^2)^4} \right] \\ \chi &= \chi_\nu + \chi_e \\ \chi_\nu &= qN \frac{\alpha}{n(\omega_0^2 - \omega^2)} \\ \alpha &= qN \frac{\omega_0^2 (n_\nu^2 - 1)}{4\pi q N} \end{aligned} \quad (14)$$

The coefficient of the thermal expansion of condensed matter is given by

$$\alpha_T = -\frac{ak_B}{m\omega_0^4 a_1} \quad (15)$$

The main idea was to derive a formula for the coefficient of the nonlinear refractive index using a simple model of the interaction of matter and light. The potential energy function of the vibrational mode can be written as

$$U(x) = \frac{\omega_0^2 m}{2} x^2 + \frac{\beta m}{3} x^3 + \frac{\gamma m}{4} x^4 \quad (16)$$

The probability of the displacement of the ion from its equilibrium position is given by

$$f(x) = A e^{-\frac{U(x)}{k_B T}} = A e^{-\frac{\omega_0^2 m x^2}{2 k_B T} + \frac{\beta m x^3}{3 k_B T} + \frac{\gamma m x^4}{4 k_B T}} \quad (17)$$

The average deviation of the ion from its equilibrium position in thermal equilibrium

$$\bar{x} = \frac{\int x f(x) dx}{\int f(x) dx} = \frac{\beta k_B T}{m \omega_0^4} \quad (18)$$

The thermal expansion length can then be written as

$$\begin{aligned} L(T) &= L_0(1 + \alpha_T T), \alpha_T = \frac{\bar{x}}{a_l T} \\ \alpha_T &= \frac{\beta k_B}{m \omega_0^4 a_l} \rightarrow \beta = \frac{m \omega_0^4 a_l}{k_B} \alpha_T \end{aligned} \quad (19)$$

The term β can then be written in terms of the thermal expansion coefficient α_T as

$$\alpha_T = \frac{\beta k_B}{m \omega_0^4 a_l} \rightarrow \beta = \frac{m \omega_0^4 a_l}{k_B} \alpha_T \quad (20)$$

On substituting this expression of β in Eq. D, and considering the non-resonant response ($\omega \ll \omega_0$), we get the vibrational contribution to n_2 at THz frequencies given by

$$\bar{n}_{2,\nu} = \bar{n}_{2,\nu}^{(1)} + \bar{n}_{2,\nu}^{(2)} = \frac{3a_l^2 m^2 \omega_0^4 \alpha_T^2}{32n_0 \pi^2 q^2 N^2 k_B^2} [n_{0,\nu}^2 - 1]^3 - \frac{9}{32\pi N n_0 \hbar \omega_0} [n_{0,\nu}^2 - 1]^2 \quad (21)$$

The following parameters are included in the expression: a_l is the dimension of unit cell; m is the reduced mass of the vibrational mode, ω_0 is the fundamental vibrational frequency, α_T is the thermal expansion coefficient. The parameter q is the effective charge of the chemical bond; for simplicity, this value was taken to be equal to the charge of the electron. N is the density of the number of vibrational units, which is given by the ratio of the specific gravity of the liquid and the molecular mass. For water, the specific gravity is 1 g/cm³, and its molecular mass is 18 amu (1.67×10^{-24}), which gives a number density of 3.3×10^{22} per 1 cm⁻³. We also define $n_{0,\nu}$ as the vibrational contribution to the low-frequency refractive index as

$$n_{o,\nu} = \sqrt{1 + n_0^2 - n_{el}^2}, \quad (22)$$

where n_0 is the linear refractive index in THz region, n_{el} is refractive index in the range with nonresonant electronic contribution.

The mathematical model of a liquid used above, based on a model of a molecule in the form of an anharmonic oscillator, is of course very simplified. Its role is to express the desired value n_2 of the material in terms of other physical characteristics of the liquid, which, importantly, should have been obtained in the framework of the SAME simple model of the molecule and the method of averaging its response over an ensemble of molecules. In fact, the resulting formula n_2 of the material with this approach should be considered semi-heuristic. But a comparison of the results of theory and experiment shows good agreement, which in our opinion confirms the validity of the approach proposed in [3].

E. Dispersion of the nonlinear refractive index coefficient in the THz spectral range for water

As was shown in previous theoretical works [3, 4], the dispersion of the nonlinear refractive index of vibrational nature can be regarded as constant between 0 and 5 THz. The dispersion of the nonlinear refractive index coefficient is expected to become notable when approaching two-photon resonance with the fundamental vibrational mode (i.e., stretching vibration of water molecule). The fundamental vibrational mode corresponds to 100 THz for water.

We calculate the value of n_2 in the spectral range of 0.3 to 3.5 THz using the following expression [3, 4]:

$$\bar{n}_{2,\nu} = \bar{n}_{2,\nu}^{(1)}(0) \frac{1}{n(\omega)/n(0)} \cdot \frac{1 - 8 \left(\frac{\nu}{\nu_0} \right)^2}{\left(1 - \left(\frac{\nu}{\nu_0} \right)^2 \right)^4 \left(1 - \left(2 \frac{\nu}{\nu_0} \right)^2 \right)} - \bar{n}_{2,\nu}^{(2)}(0) \frac{1}{n(\omega)/n(0)} \cdot \frac{1}{\left(1 - \left(\frac{\nu}{\nu_0} \right)^2 \right)^4} \quad (23)$$

where $n(\omega)$ is a linear refractive index dispersion in THz range taken from [5]. The central frequency of the THz spectrum used in the experiments (0.75 THz) was chosen as $n_2(0)$ and $n(0)$ values. Fig. S7 shows the value of n_2 calculated over the aforementioned spectral range.

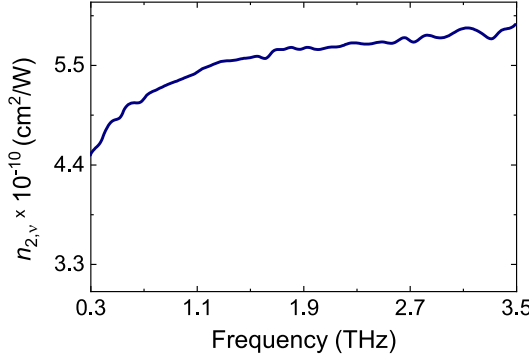


FIG. S7. Dispersion of n_2 in the terahertz frequency range for water.

As can be seen from the figure above, the value of n_2 varies from 4.4×10^{-10} to $5.7 \times 10^{-10} \text{ cm}^2/\text{W}$, whereas the value of n_2 of water calculated from the equation (2) in the main text is $5 \times 10^{-10} \text{ cm}^2/\text{W}$. Since the variation in n_2 in the spectral range of interest is within 15 % of the value predicted by our theoretical model, we can assume n_2 to be dispersionless for simplicity. We further note that this variation in n_2 falls within the range of error in the estimation of n_2 from our z-scan traces.

F. Comparison of the contributions of different mechanisms to the nonlinearity

Here we calculate and compare the contributions of the various mechanisms other than the molecular vibrational response to the nonlinear refractive index coefficient of water. The nonlinear refractive index due to molecular orientation is given by [6]

$$\bar{n}_2 = \frac{N}{45n_0} \left(\frac{n_0^2 + 2}{3} \right)^4 \frac{(\alpha_3 - \alpha_1)^2}{kT} \quad (24)$$

where N is the number density of molecules, α_3 denotes the polarizability experienced by an optical field that is polarized parallel to the symmetry axis, α_1 denotes the polarizability experienced by a field that is polarized perpendicular to its symmetry axis, T is the temperature and k is the Boltzmann constant.

Substituting the parameters $N = 3 \times 10^{22} \text{ cm}^{-1}$, $n_0 = 1.33$, $\alpha_3 = 1.86 \text{\AA}^3$ [7], $\alpha_1 = 1.63 \text{\AA}^3$ [7], and $T = 293.15 \text{ K}$, in the above equation, we find that $\bar{n}_2 = 1.6 \times 10^{-15} \text{ esu}$, which gives the value of n_2 as $6.9 \times 10^{-18} \text{ cm}^2/\text{W}$.

The electronically induced change in the refractive index in THz frequency range is determined by the value of n_2 in the NIR range [8], which is $1.9 \times 10^{-16} \text{ cm}^2/\text{W}$.

To estimate the thermal contribution to n_2 , we use the following expression for a cw beam [6]

$$n_2^{th} = \left(\frac{dn}{dT} \right) \frac{\alpha R^2}{k} \quad (25)$$

Here (dn/dT) denotes the temperature coefficient of the refractive index, α denotes the linear absorption coefficient of the material, k denotes the thermal conductivity, and R is a radius of a circular laser beam (hereafter the formulas are taken from [6]).

Substituting the parameters $(dn/dT) = -9.5 \times 10^{-5} \text{ K}^{-1}$ [9], $\alpha = 200 \text{ cm}^{-1}$ [10], $\kappa = 0.595 \text{ W}/(\text{m} \times \text{K})$ [9], and $R = 0.5 \text{ mm}$, in the above equation, we get $n_2^{(th)} = 8 \times 10^{-3} \text{ cm}^2/\text{W}$.

The response time τ_r for the thermal nonlinearity is given by

$$\tau_r \approx \frac{(\rho_0 C)R^2}{\kappa} \quad (26)$$

Substituting the same parameters as above, we find that $\tau_r \approx 1.75 \text{ s}$. The water jet used in the experiments has a speed of $v_{jet} = 1 \text{ m/s}$, which implies that the geometric interaction area between the jet and the THz beam changes

faster than the time it would take for the thermal effects to build up. Since the accumulation of the thermal effect can be considered to be linear, and that the interaction of the jet with the beam occurs for about 1 ps (10^{-12} s), the thermal contribution is about 10^{-14} cm²/W.

- [1] D. A. Kislin, M. A. Knyazev, Y. A. Shpolyanskii, and S. A. Kozlov, Self-action of nonparaxial few-cycle optical waves in dielectric media, *JETP Letters* **107**, 753 (2018).
- [2] M. Sheik-Bahae, A. Said, T.-H. Wei, D. Hagan, and E. V. Stryland, Sensitive measurement of optical nonlinearities using a single beam, *IEEE Journal of Quantum Electronics* **26**, 760 (1990).
- [3] K. Dolgaleva, D. V. Materikina, R. W. Boyd, and S. A. Kozlov, Prediction of an extremely large nonlinear refractive index for crystals at terahertz frequencies, *Physical Review A* **92**, 10.1103/physreva.92.023809 (2015).
- [4] S. A. Kozlov, A. A. Drozdov, K. Dolgaleva, and R. W. Boyd, Nonlinear refractive index for crystals at terahertz frequencies (invited paper), in *2015 40th International Conference on Infrared, Millimeter, and Terahertz waves (IRMMW-THz)* (2015) pp. 1–3.
- [5] T. Bowman, M. El-Shenawee, and L. K. Campbell, Terahertz transmission vs reflection imaging and model-based characterization for excised breast carcinomas, *Biomed. Opt. Express* **7**, 3756 (2016).
- [6] R. W. Boyd, Ultrafast and intense-field nonlinear optics, in *Nonlinear Optics* (Elsevier, 2008) pp. 561–587.
- [7] X. Ge and D. Lu, Molecular polarizability of water from local dielectric response theory, *Physical Review B* **96**, 10.1103/physrevb.96.075114 (2017).
- [8] Z. Wilkes, S. Varma, Y.-H. Chen, H. Milchberg, T. Jones, and A. Ting, Direct measurements of the nonlinear index of refraction of water at 815 and 407 nm using single-shot supercontinuum spectral interferometry, *Applied Physics Letters* **94**, 211102 (2009).
- [9] N. Arnaud and J. Georges, Investigation of the thermal lens effect in water–ethanol mixtures: composition dependence of the refractive index gradient, the enhancement factor and the soret effect, *Spectrochimica Acta Part A: Molecular and Biomolecular Spectroscopy* **57**, 1295 (2001).
- [10] D. K. George and A. G. Markelz, Terahertz spectroscopy of liquids and biomolecules, in *Terahertz Spectroscopy and Imaging* (Springer Berlin Heidelberg, 2012) pp. 229–250.